*Manuscript submitted to the Journal of Sedimentary Research*
*as a "Current Ripple", January, 2005*

# EXPERIMENTS ON SELF-CHANNELIZED SUBAQUEOUS FANS EMPLACED BY TURBIDITY CURRENTS

BIN YU[1*], ALESSANDRO CANTELLI[1], JEFF MARR[1], CARLOS PIRMEZ[2], CIARÁN O'BYRNE[2] AND GARY PARKER[1]

[1]*St. Anthony Falls Laboratory, University of Minnesota, Minneapolis, MN 55414 USA*

*e-mail: parke002@umn.edu*

[2]*Shell International Exploration and Production Inc.3737 Bellaire Blvd., Houston, TX 77025, USA*

**ABSTRACT: The passage of turbidity currents over submarine fans often results in intense channelization. The channels are typically bounded by levees, and vary from mildly to strongly meandering. The process of self-channelization remains, however, somewhat obscure. Preliminary experiments reported here demonstrate for the first time that self-channelization of subaqueous fans by turbidity currents can be reproduced at laboratory scale. The resulting weakly sinuous channels can be predominantly depositional, predominantly erosional or some combination of the two. The channels can elongate to the length of the entire reach available for their formation. They can show both gradual shift and avulsion. Two necessary conditions for the formation of intense channelization appear to be a) a multiplicity of grain sizes and b) a turbidity current that is insufficient to cover the entire area of the fan at any given time. Field analogs to the experimental channelized fans can often be found at the distal end of submarine fans. An example from the Gulf of Cadiz is cited.**

*Present Address: Institute of Mountain Hazards and Environment, Chinese Academy of Science, PO Box 417, Chengdu 610041, China, drbinyu@yahoo.com

## INTRODUCTION

Submarine fans constitute major deep-water sinks for terrestrial sediments brought across the continental shelf and slope. Many such fans are intensely channelized; the channels are often strongly meandering and bounded by well-developed levees. Examples of channelized submarine fans include the Amazon Submarine Fan (Pirmez 1994, Pirmez and Flood 1995), the Mississippi Submarine Fan (Twitchell et al. 1991) and the Bengal Fan (Schwenck et al. 2003). A levee-bounded meandering channel on the Amazon Submarine Fan is shown in Fig. 1.

Meandering channels on submarine fans are created by the passage of turbidity currents. The process by which a turbidity current flowing over an initially featureless surface self-channelizes so as to create a distributary network of sinuous leveed channels remains only partially understood. Here preliminary results demonstrate for the first time that turbidity currents at experimental scale can deposit subaqueous fans that are intricately channelized by low-relief, mildly sinuous channels.

## EXPERIMENTAL SETUP AND PROCEDURE

The experimental effort reported here is an outgrowth of an accident that occurred in the late 1990's. Marr et al. (2001; see also Marr, 1999) conducted a set of experiments on subaqueous debris flows in a channel with a width of 0.20 m and a length of 10 m. In one of those experiments a mixture of sand and bentonite clay was used to form the slurry of the debris flow. The slurry was released by opening the gate of a head tank; the resulting debris flow traversed the length of the channel and produced a deposit in less than a minute. Evidently a small amount of bentonite-rich slurry was retained in the head tank, however. This slurry leaked out slowly as a turbidity current overnight. By the next morning this had resulted in the formation of several small, sinuous leveed channels (Fig. 2). These channels showed a clear resemblance to field-scale analogs on submarine fans, variously displaying distal lobes, levee overflow splays and incipient avulsions. Since the formation of these “accidental” channels had not been expected, however, the formative process was not observed. A further accident caused the tank containing the deposit to drain abruptly, so obliterating the channels before they could be fully documented. The conditions under which they formed remained a mystery. The program of experimentation reported here was motivated by the desire to explain that mystery.

The experiments reported here were conducted in a small rectangular basin at St. Anthony Falls Laboratory, University of Minnesota. The experimental setup is illustrated in Fig. 3. The basin is 3.9 m long, 2.15 m wide and 0.6 m deep. Turbidity currents were introduced into the basin from the left-hand side of Fig. 3; in subsequent text this side is referred to as the upstream side, and the opposite side the downstream side. The basin contains a movable steel platform with a length of 3.3 m and a width equal to that of the entire basin. This platform was set to a slope of 7.0 percent (4.0°) for all the experiments reported here. At the downstream end of the steel surface is a vertical ledge with a drop of 0.05 m, beyond which the basin extends for another 0.6 m.

The basin was filled with tap water to a depth of 0.57 m for the experiments. This depth ensured that the upstream (left) end of the steel platform of Fig. 3 was submerged below 0.289 m of water for all the experiments. As successive experiments were run over the deposits of previous experiments, the minimum depth of submergence of the deposit decreased in time. This minimum depth was, however, never less than 0.1 m. Turbid water was introduced into the basin from a cylindrical mixing tank with a volume of 189 liters (50 gallons) placed above upstream end of the basin (Fig. 3). Water and sediment were introduced into the mixing tank, thoroughly mixed by hand, and then introduced into the basin by means of a pipe with an inner diameter of 16 mm. The flow rate in the pipe was adjusted with a valve. For any valve setting the discharge of slurry into the tank decreased in time as the head difference between the mixing tank and the basin declined. The discharge values reported below are averages determined from the rate of fall of the free surface in the mixing tank. The flow (and thus the run) was terminated when the total volume of water and sediment remaining in the mixing tank declined to between 10 to 30 percent of the initial value.

Scores of trial experiments were conducted in order to delineate the conditions for the 14 experiments of Table 1. In the experiments of Table 1, the volume concentration of sediment in the slurry in the head tank was always set to 10 percent. The sediment was composed of a mixture of four sediment types: a) kaolinite clay, b) silica flour with a nominal size of 20 $\mu$m, c) silica flour with a nominal size of 45 $\mu$m and d) silica flour with a nominal size of 110 $\mu$m. The grain size distributions of these are shown in Fig. 4. The specific gravity of the silica flour was 2.60; that of the kaolinite is presumably near 2.65. In the trial experiments preceding those of Table 1, clearly formed channels were not obtained using only one of these four sediment types. The proportions of the four sediment types were thus varied from experiment to experiment to determine optimal conditions for channelization. The proportions of sediment type used in the runs of Table 1 all fall within the range for which good channel formation was observed.

The slurry was introduced into the tank from a flexible pipe at a point at the transversal center of the basin and 15 - 20 cm downstream of the upstream wall. Over time the slurry deposited out to form the caldera-like feature of Fig. 5. The slurry overflowed the caldera to form a spreading turbidity current that deposited the subaqueous fan. As sediment deposited out the flexible pipe was gradually raised to prevent burial.

During experiments turbid water was removed via a bottom drain at the downstream end of the tank; fresh water was added at level of the water surface at the downstream end so as to maintain a constant water surface elevation and a constant, small overflow of water over a weir at the downstream end. This configuration reduced, but by no means prevented, the pollution of the ambient sediment-free water by the turbidity current as each experiment proceeded.

It is seen in Table 1 that for the 14 experiments reported here, average discharge varied between 0.015 and 0.05 liters/s; total initial volume in the head tank varied between 37.8 liters to 189 liters. The fractions of nominal 45 μm and 110 μm silica flour were held constant at 0.15 and 0.05 by weight respectively (except for one experiment, where the fraction of 45 μm silica flour was lowered to 0.10 by weight), and the fraction clay was varied from 0.20 to 0.60 by weight. Each experiment lasted between 15 and 75 minutes. The deposit of each experiment formed on top of that of the preceding experiment of Table 1; the steel platform was not cleaned between runs. Two or three hours were required after each run to allow the water to clarify and make the resulting deposit visible.

Data acquisition was rather limited due to the exploratory nature of these experiments. The flows themselves were recorded by means of videotape. The deposits were thoroughly documented photographically. In order to highlight topography of the experimental subaqueous fans, after completing the experiment a very low discharge of a saline solution containing red dye was released from the caldera and allowed to flow freely across the fan. Occasional spot measurements of bed elevations were taken.

## EXPERIMENTAL RESULTS

## Conditions for Channelization

While the overflow caldera of Fig. 5 may not be representative of the typical upstream end of submarine channels in the field, it nevertheless represented an excellent way to study the controls on channelization of subaqueous fans overridden by turbidity currents. As the slurry from the head tank plunged into the caldera, it was observed to copiously entrain ambient clear water into it. At it overflowed the rim of the caldera, it formed a well-defined turbidity current. A possible analogy is that of a submarine avulsion, where turbidity currents breach a pre-existing channel and flow down the backside of the levee (e.g. Pirmez and Flood, 1995). It should be noted that the discharges of Table 1 are all very small. These small discharges were obtained as a result of the preceding trial experiments. When the overflow discharge was sufficiently high, the turbidity current tended to spread uniformly across the platform, inundating the entire subaqueous fan and creating a featureless deposit obeying approximate radial symmetry. The thickness of the deposit decreased downstream, but showed virtually no variation in the axial direction, and in particular no evidence of channelization. When the overflow discharge was sufficiently low, however, the turbidity current could cover no more than a fraction of the fan surface at any given instant. As a result the turbidity current repeatedly shifted its depocenter in the axial direction in erratic ways, often leaving channels behind.

Run 6 provides an example of this. Fig. 6a shows the turbidity current exiting the caldera through a breach. It can be seen that the turbidity current covers only a portion of the subaqueous fan. The erosional channel created by the breach is shown in Fig. 6b. A panoramic view of the subaqueous fan after the end of Run 6 is given in Fig. 6c. The erosional channel is seen at the upstream end of the image, and several net-depositional leveed channels are seen farther downstream. Two of these leveed channels are seen in more detail in Fig. 6d. The upper channel ends in a depositional lobe. The lower channel shows a series of side lobes deposited by overflow. The dark area in between the channels defines an inter-channel low.

It should be pointed out that breaching of the caldera was not a necessary condition for the formation of either net-erosional or net-depositional channels. In many cases either or both of these formed downstream of the caldera rim with no obvious breach. In all cases, however, the turbidity current was insufficient to cover more than about half of the fan surface at any given time.

**Net-depositional leveed channels**

Leveed channels can be seen in more detail in Fig. 7, which is a photomosaic of part of the downstream end of the fan produced in Run 1. Toward the downstream end of the image four leveed channels (two of which form from a channel bifurcation) and three inter-channel troughs are visible in the figure. The channels are seen to be weakly sinuous. Although not shown in Fig. 7, they extended over the entire 3.3 m length of the basin, from just below the rim of the upstream caldera to the dropoff ledge of Fig. 3, which can also be seen in Fig. 7. Channel widths were in the range 15 - 30 mm. Levee height from either the bare steel surface or an inter-channel depression was on the order of 3 – 5 mm. The difference in elevation between the top of the levee and the channel bottom could not easily be measured without disturbing the deposit, but was on the order of 1 – 2 mm.

It was quite common for leveed channels to traverse the entire fan, all the way to the downstream ledge during a single experiment. Preserved distal channel lobes such as the one of Fig. 6d were more the exception rather than the rule.

**Channelized fans**

As the deposits of runs were stacked successively one on top the other, the surface of the experimental subaqueous fan became covered by a progressively more intricate pattern of recently active and abandoned channels. Fig. 8a shows the fan topography at the end of Run 12. The fan surface is seen to be completely channelized by interwoven distributaries. The figure should be interpreted with caution for two reasons. Firstly, the darker patches in the image were created by red dye, which did not propagate to the end of the fan. Channels which appear to end on the fan in the image in fact typically extended to the downstream ledge, as in Fig 7. In addition, not all the darker areas denote recently-active channels; some denote abandoned channels and some denote inter-channel troughs. Fig. 8b. provides a detailed view of the channels at the end of Run 12 just below the caldera. It is seen in the image that channel heads are not necessarily associated with a caldera breach.

Figures 9a and 9b show photomosaics of the entire fan after the end of Runs 12 and 13, respectively. Again, red dye was used to highlight the topography. Detailed comparison of the figures shows a number of channels that have migrated, avulsed or merged. The two images provide evidence that the process of channelization on the experimental fans is a highly dynamic one. The downstream ledge of the tank (Fig. 3) is evident in both figures. It can be seen that numerous channels extend all the way to the ledge. Deposition beyond the ledge was sufficient to allow some of them to elongate beyond the ledge.

Figure 10 shows several scarps of knickpoints that formed below the rim of the caldera during Run 3. These knickpoints were common features of the experiment, and were observed to actively migrate upstream, leaving a net-erosional channel downstream. In many cases such channels metamorphosed into net-depositional leveed channels farther downstream. The knickpoints would often form, migrate upstream for a distance, disappear, and then reappear elsewhere in a cyclic pattern. A similar knickpoint that defines a channel head is visible on the right-hand side of Fig. 8b.

## INTERPRETATION

A comparison of Figs. 1, 7, 9a and 9b reveals that the experimental leveed channels which formed in the experiments are considerably less sinuous and rather more ill-defined than, for example, the major leveed channels on the Amazon Submarine Fan. This does not mean that field analogs are lacking. The distal regions of some submarine fans are often covered with intricate patterns of low-relief, low-sinuosity channels that rather more closely resemble the experimental channels reported here. For example, such channel complexes are seen in at the distal end of the Mississippi Submarine Fan (e.g. Twitchell et al. 1992) and the distal end of the Gulf of Cadiz Submarine Fan (Akhmetzhanov et al., in press). Fig. 11 shows a portion of a small fan in the Gulf of Cadiz. Although the experimental channels are not perfect analogs of those of Fig. 11, which are somewhat more sinuous, the resemblance between Fig. 11 and Figs. 7, 9a and 9b is nevertheless striking. The vast difference in scale notwithstanding, it seems reasonable to assume that the formative mechanism for the field channels is similar to that of the experimental channels.

The formative mechanism of leveed, sinuous channels has been the source of some speculation (e.g. Imran et al. 1998; Peakall et al. 2000). The experiments reported here are not as yet of sufficient detail to shed light on this issue. The fact that subaqueous leveed channels can be produced experimentally, however, offers a new avenue of research for study of the formative mechanism.

A second analogy is of interest. Fig. 12 shows a series of knickpoint-like features located near the shelf-slope break along the continental margin of Santa Barbara, California USA. These features serve as the heads of four distinct, mildly sinuous channels. A comparison of Figs. 8b, 10 and 12 reveal a clear similarity. The experiments show that a sheet-like turbidity current that is too thin to cover the entire bed surface can result in flow concentration and the formation of upstream-migrating knickpoints. These knickpoints then serve as the head of net-erosional channels, which may become net-depositional farther downstream. One possibility for the formation of the knickpoints and channels seen in Fig. 12 is that they are produced by sheet turbidity currents, perhaps generated by a storm, that overspill the shelf-slope break and lead to channelization. This possibility has been explored in more detail by Izumi (2002).

## CONCLUSION

The preliminary experiments reported here provide the first documentation for process of self-channelization on an experimental subaqueous fan. Both net-depositional channels bounded by levees and net-erosional channels, the latter often originating from headcut scarps, were produced in the experiments.

No claim is made here that the experimental channelized fans are exact, or even approximate dynamical models of their field analogs. It is suggested, however, that a) the experiments reveal a new and exciting avenue for the study of the phenomenon of self-channelization in the subaqueous setting, and b) the comparison with several field realizations is sufficiently encouraging to indicate the possibility that similar mechanisms are at work.

## ACKNOWLEDGEMENTS

This research was funded by Shell International Exploration and Production Inc. The participation of B. Yu was made possible in part by funding from the National Center for Earth-surface Dynamics, which is in turn funded by the Science and Technology Center Program of the US National Science Foundation. This paper is a contribution of the National Center for Earth-surface Dynamics, and is related to the Center mission pertaining to channels.

## REFERENCES


AKHMETZHANOV, A.M., KENYON, N.H., O'BYRNE, C.J., AND IVANOV, M.M., 2004, SPECULOBE, a high resolution study of a modern sand lobe at the end of a gravity flow channel. Geological Society of London, in press (full reference to be provided later).

IMRAN, J., PARKER, G. AND KATOPODES, N., 1998, A numerical model of channel inception on submarine fans: Journal of Geophysical Research Oceans, v. 103(C1), p. 1219-1238.

IZUMI, N., 2002, Theory of the formation of submarine canyons due to turbidity currents: Japan Society of Civil Engineers Journal of Hydraulic, Coastal and Environmental Engineering, v. 712(II-60), p. 45-56.

MARR, J.D.G., 1999, Experiments on subaqueous sandy gravity flows: flow dynamics and deposit structures: M.S. thesis, University of Minnesota, Minneapolis, 121 p.

MARR, J.D., HARFF, P., SHANMUGAM, G., AND PARKER, G., 2001, Experiments on subaqueous sandy gravity flows: the role of clay and water content in flow dynamics and depositional structure: Geological Society of America Bulletin, v. 113(10), p. 1377-1386.

PEAKALL, J., MCCAFFREY, W.D., AND KNELLER, B.C., 2000, A process model for the evolution, morphology and architecture of meandering submarine channels: Journal of Sedimentary Research, v. 70, p. 434-448.

PIRMEZ, C., 1994, Growth of a submarine meandering channel-levee system on Amazon Fan: Ph.D. thesis, Columbia University, New York, 587 p.

PIRMEZ, C., AND FLOOD, R.D., 1995, Morphology and structure of Amazon channel: In; Flood, R.D., Piper, D.J.W., Klaus, A., et al. (Eds.), Proceedings of the ODP, Initial Reports, 155, Ocean Drilling Program, College Station, TX, p. 23-45.

SCHWENCK, T., SPEIß, V., HÜBSCHER, C. AND BREITZKE, M., 2003, Frequent channel avulsions within the active channel-levee system of the middle Bengal Fan-an exceptional channel-levee development derived from Parasound and Hydrosweep data: Deep-Sea Research II, v. 50, p. 1023-1045.

TWICHELL, D.C., KENYON, N.H., PARSON, L.M., AND MCGREGOR, B.A., 1991, Depositional patterns of the Mississippi Fan surface: Evidence from GLORIA II and high-resolution seismic profiles: in Weimer, P. and Link, M.H., eds., Seismic Facies and Sedimentary Processes of Modern and Ancient Submarine Fans: Springer-Verlag, New York, NY, p. 349-364.

TWICHELL, D.C., SCHWAB, W.C., NELSON, C.H., LEE, H.J., AND KENYON, N.H., 1992, Characteristics of a sandy depositional lobe on the outer Mississippi Fan from SeaMARC IA sidescan sonar images: Geology, v. 20, p. 689-692.

Table 1. Experimental parameters

| Run | Discharge (liters/s) | Total volume in head tank (liters) | Fraction Clay | Fraction Silica (20μm) | Fraction Silica (45μm) | Fraction Silica (110μm) |
|---|---|---|---|---|---|---|
| 1 | 0.04 | 189 | 0.40 | 0.40 | 0.15 | 0.05 |
| 2 | 0.04 | 189 | 0.40 | 0.40 | 0.15 | 0.05 |
| 3 | 0.04 | 94.5 | 0.40 | 0.40 | 0.15 | 0.05 |
| 4 | 0.05 | 151.2 | 0.30 | 0.50 | 0.15 | 0.05 |
| 5 | 0.05 | 75.6 | 0.30 | 0.50 | 0.15 | 0.05 |
| 6 | 0.05 | 189 | 0.30 | 0.50 | 0.15 | 0.05 |
| 7 | 0.05 | 113.4 | 0.30 | 0.50 | 0.15 | 0.05 |
| 8 | 0.025 | 189 | 0.20 | 0.60 | 0.15 | 0.05 |
| 9 | 0.025 | 75.6 | 0.50 | 0.30 | 0.15 | 0.05 |
| 10 | 0.025 | 75.6 | 0.60 | 0.25 | 0.10 | 0.05 |
| 11 | 0.015 | 75.6 | 0.50 | 0.30 | 0.15 | 0.05 |
| 12 | 0.026 | 75.6 | 0.50 | 0.30 | 0.15 | 0.05 |
| 13 | 0.04 | 37.8 | 0.50 | 0.30 | 0.15 | 0.05 |
| 14 | 0.03 | 37.8 | 0.50 | 0.30 | 0.15 | 0.05 |

FIGURE CAPTIONS

Figure 1. Side-scan sonar image of a meandering, leveed channel on the Amazon Submarine Fan. The turbidity current that created the channel flowed from left to right. Channel width is on the order of 2 km. From Pirmez (1994).

Figure 2. View of several small, sinuous leveed channels produced inadvertently in the course of the experiments of Marr (1999) and Marr et al. (2001). The flow was from left to right. The width of the bentonite-covered bed over which the channels formed was 0.20 m (top clear plastic wall to bottom clear plastic wall).

Figure 3. Schematic diagram of the basin where the experiments were performed.

Figure 4. Grain size distributions of the four sediment types used in the experiments.

Figure 5. View looking downward at the caldera which formed at the point where slurry exited from the flexible pipe into the basin. The image is from Run 13 of Table 1. The flow, which was turned off before taking the image, emanated from the pipe from top to bottom. The caldera was still submerged at the time the image was taken. The dark material ponded in the caldera is red saline dye. The flow spilled over the caldera in all directions, but rarely inundating the entire rim at any given time. The dimensions of caldera are approximately 100 mm in the transverse direction and 150 mm in the streamwise direction.

Figure 6. a) View of the turbidity current breaching the caldera in Run 6. Flow is from left to right.

b) View of the breached caldera and net-erosional channel at the end of Run 6. Flow was from left to right. The areas of darker shading denotes zones occupied by a red saline dye used to highlight bed topography.

c) Panoramic view looking upstream at the submarine fan after the end of Run 6. Flow was from top to bottom. The net-erosional channel of Fig. 6b is also visible in Fig. 6c. Several net-depositional leveed channels can be seen farther downstream.

d) Detailed view of two net-depositional leveed channels at the end of Run 6. The flow was from left to right. The upper channel ends in a distal lobe. The lower channel, which has a width of about 15 mm, has a series of overflow lobes deposited across its lower levee. The dark region between the channels is an inter-channel depression.

Figure 7. Photomosaic showing of four net-depositional leveed channels and three inter-channel depressions formed toward the downstream end of the fan in Run 1. The transect from A to B highlights the topography on the image. The channels are seen to run right off the ledge at the downstream end of the steel platform. Channel widths are on the order or 15 - 30 mm. The streamwise length of fan shown in the image is about 2 m.

Figure 8. a) View of the intricate topography associated with channelization of the fan evident at the end of Run 12. Flow was from top to bottom. The width of the basin is 2.15 m.

b) Closeup view of the channels just below the overflow caldera at the end of Run 12.

Figure 9. a) Photomosaic of the entire fan surface after the end of Run 12.

b) Photomosaic of the entire fan surface after the end of Run 13. A comparison of Figures 9a and 9b reveals the degree to which the channelized surface is reworked from run to run.

Figure 10. Images of scarps of upstream-migrating knickpoints formed below the rim of the caldera during Run 3.

Figure 11. Side-scan sonar image of the distal end of the fan complex of the Gulf of Cadiz Submarine Fan. Note the multitude of mildly sinuous, low-relief leveed channels. The flow direction was from right to left of the image. Image courtesy of Andrey Akhmetzhanov and Neil Kenyon (final approval pending).

Figure 12. Knickpoint-like features associated with the Arguello Canyon System observed near the continental shelf-slope break off Santa Barbara, California. The channels are oriented in the offshore direction (toward bottom left). Image courtesy Monterey Bay Aquarium Research Institute.

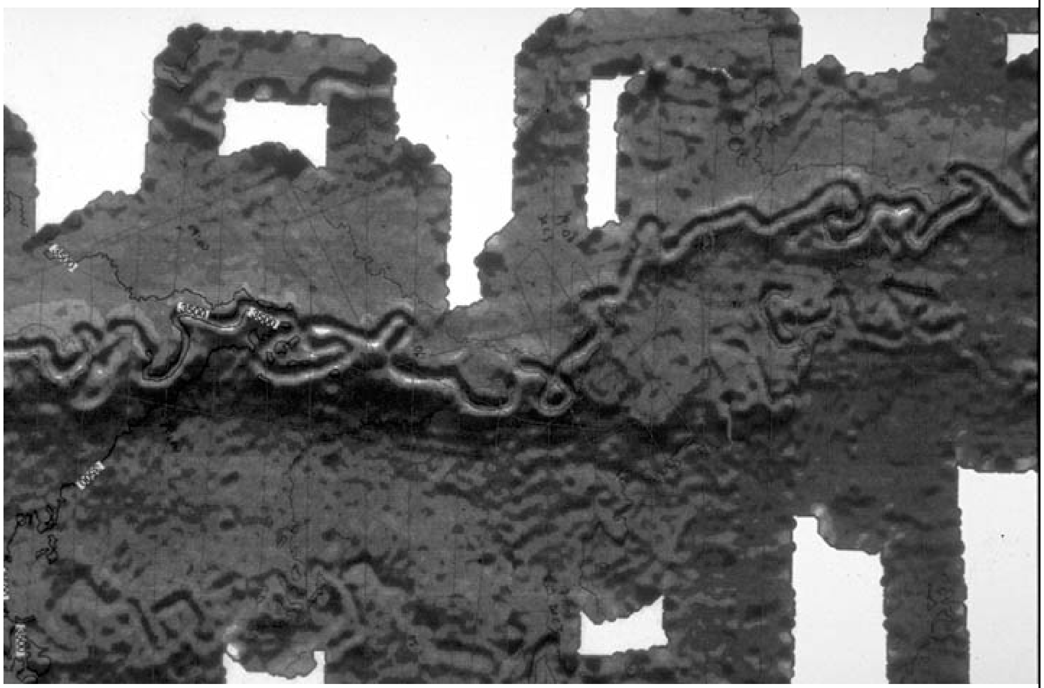

Figure 1

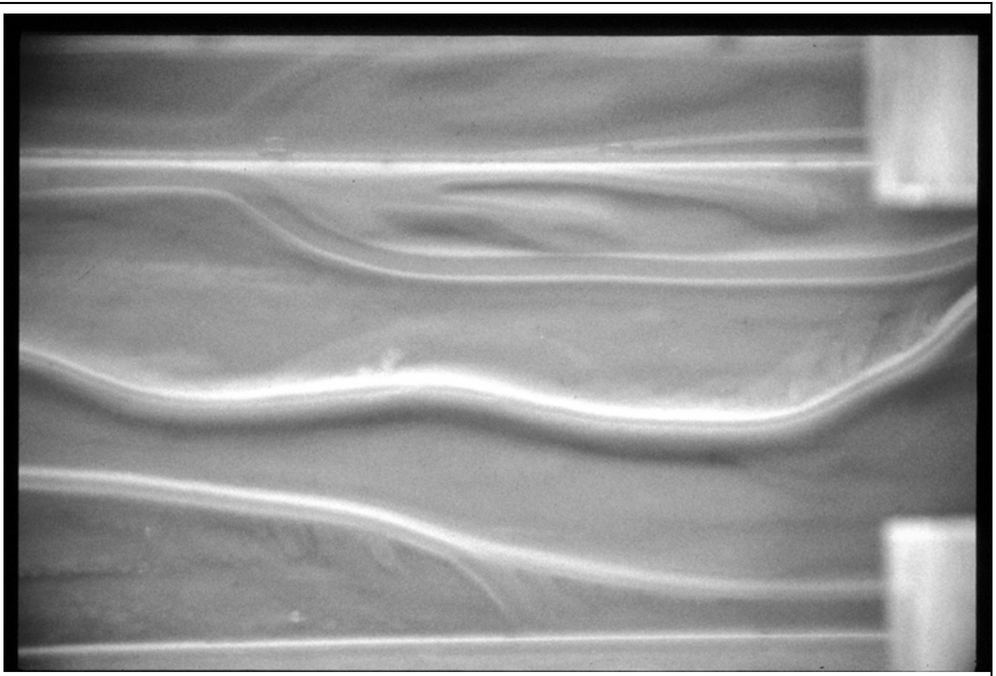

Figure 2

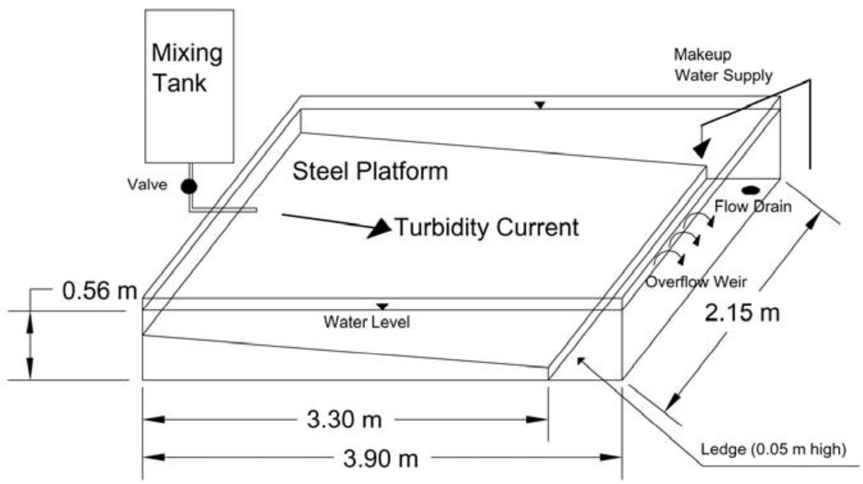


Figure 3

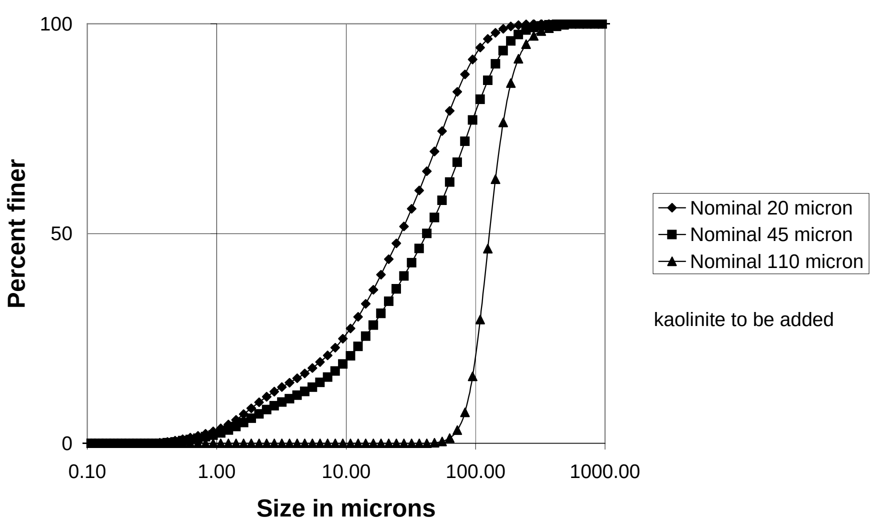


Figure 4

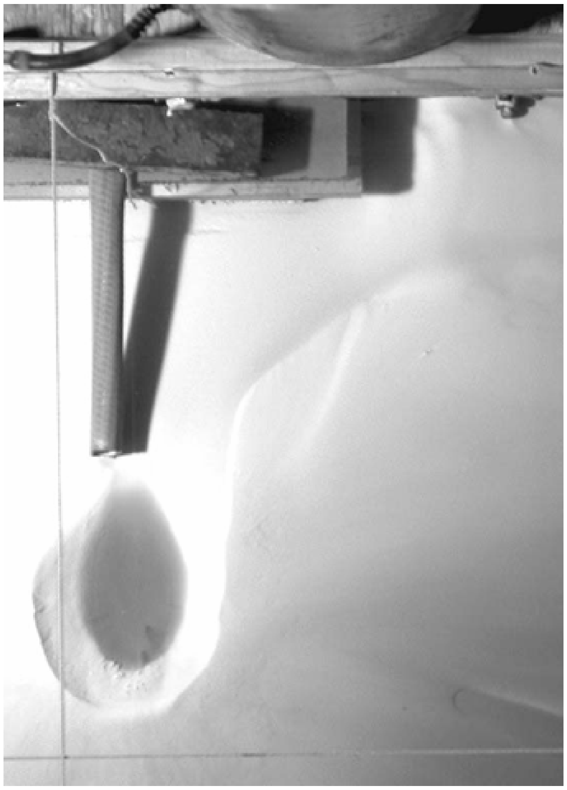

Figure 5

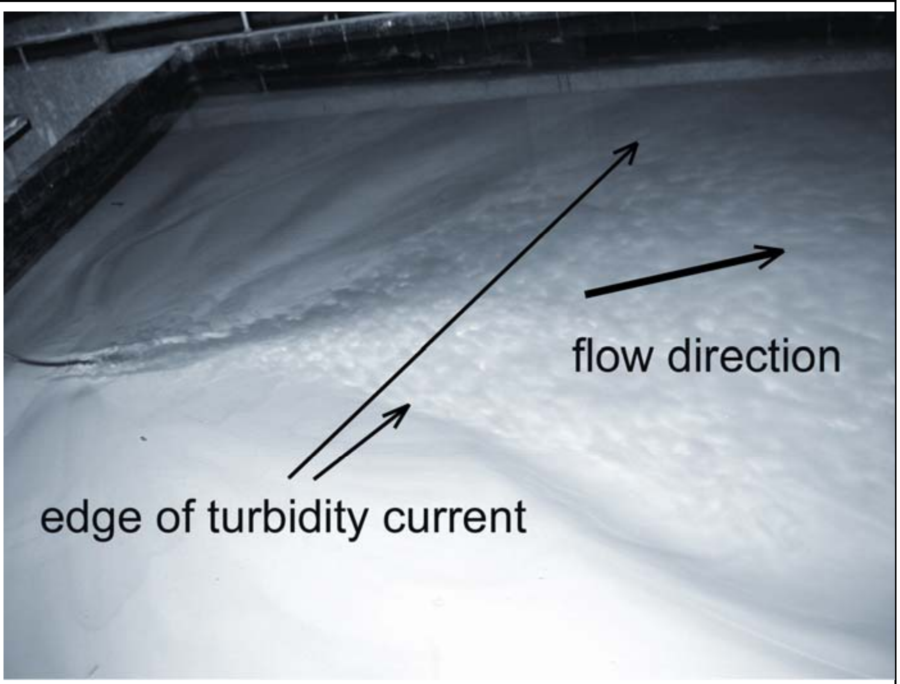


Figure 6a

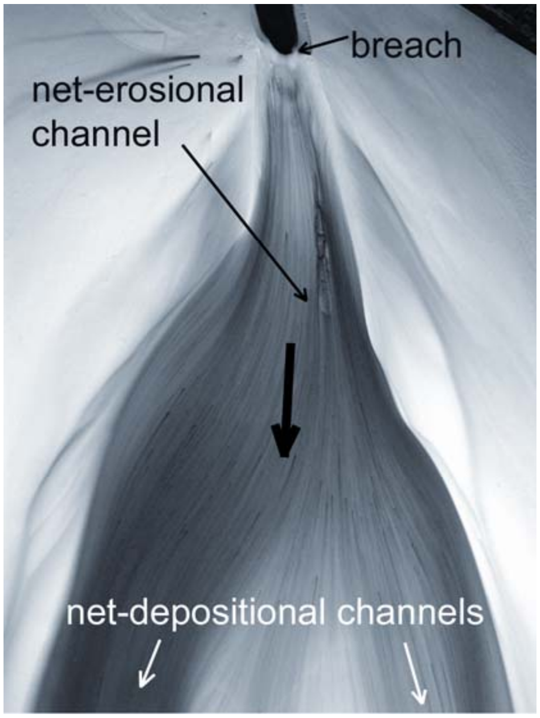


Figure 6b

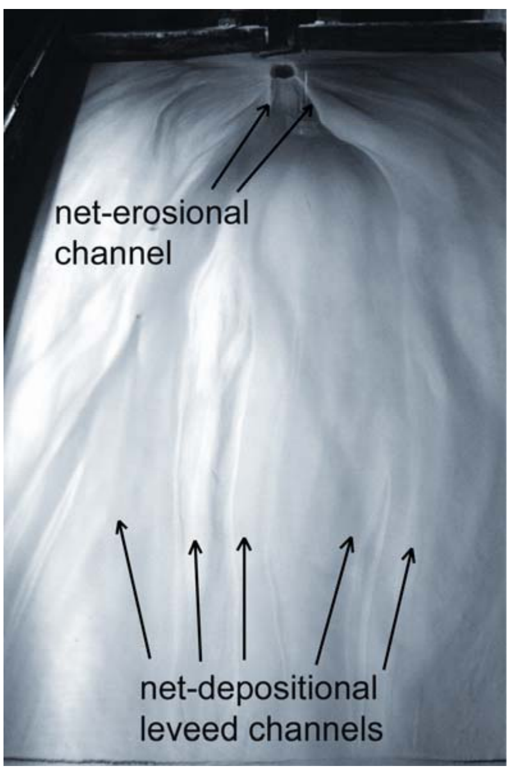


Figure 6c

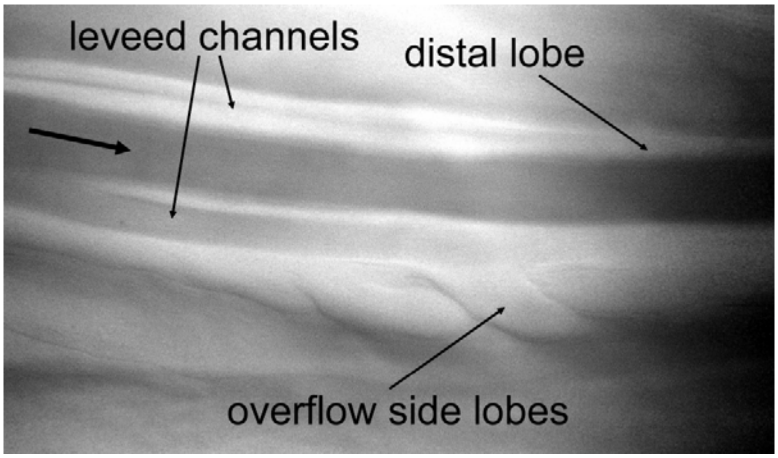

Figure 6d

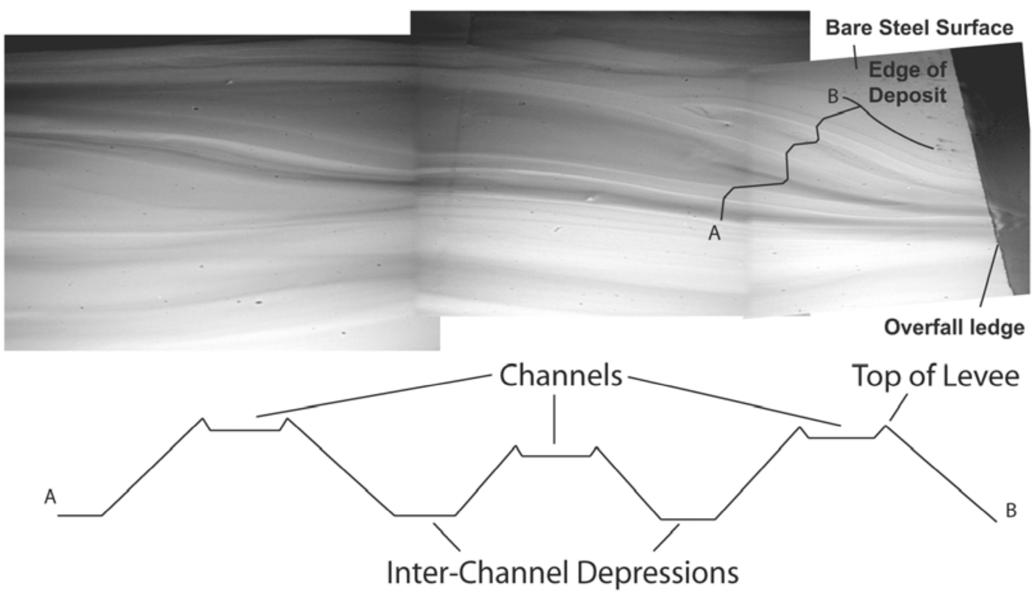

Figure 7

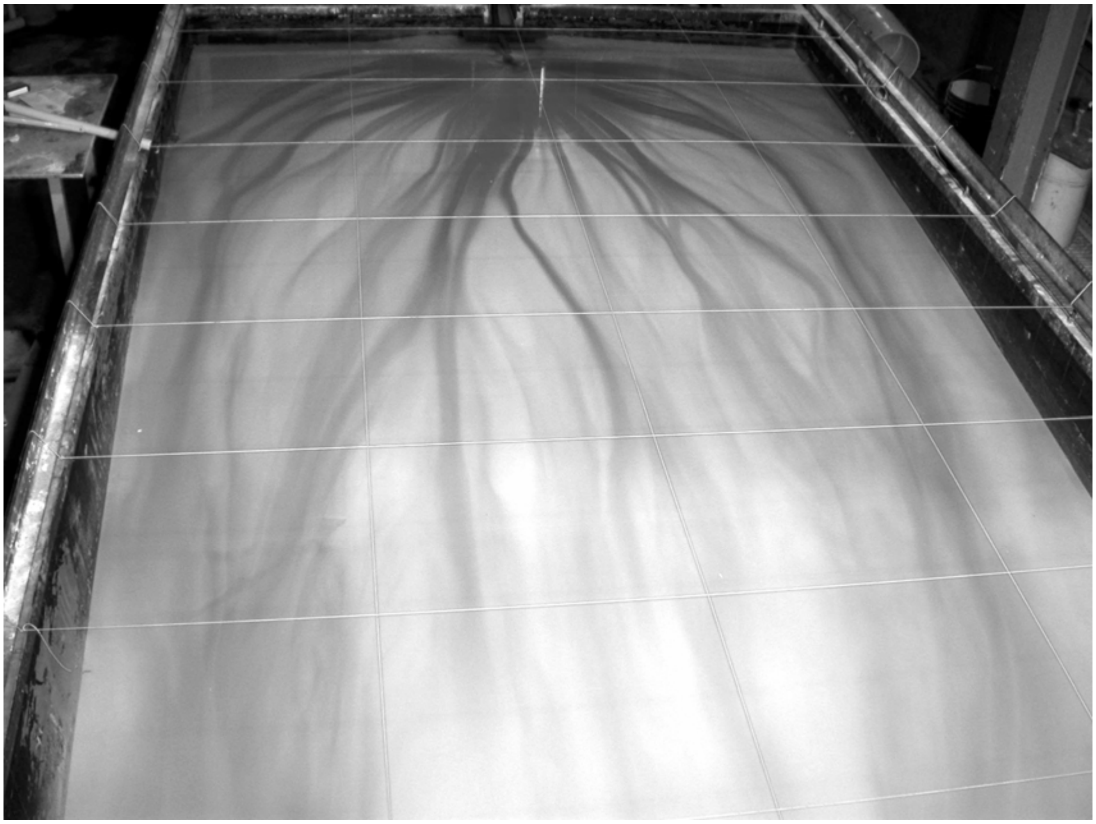
Figure 8a


Figure 8b

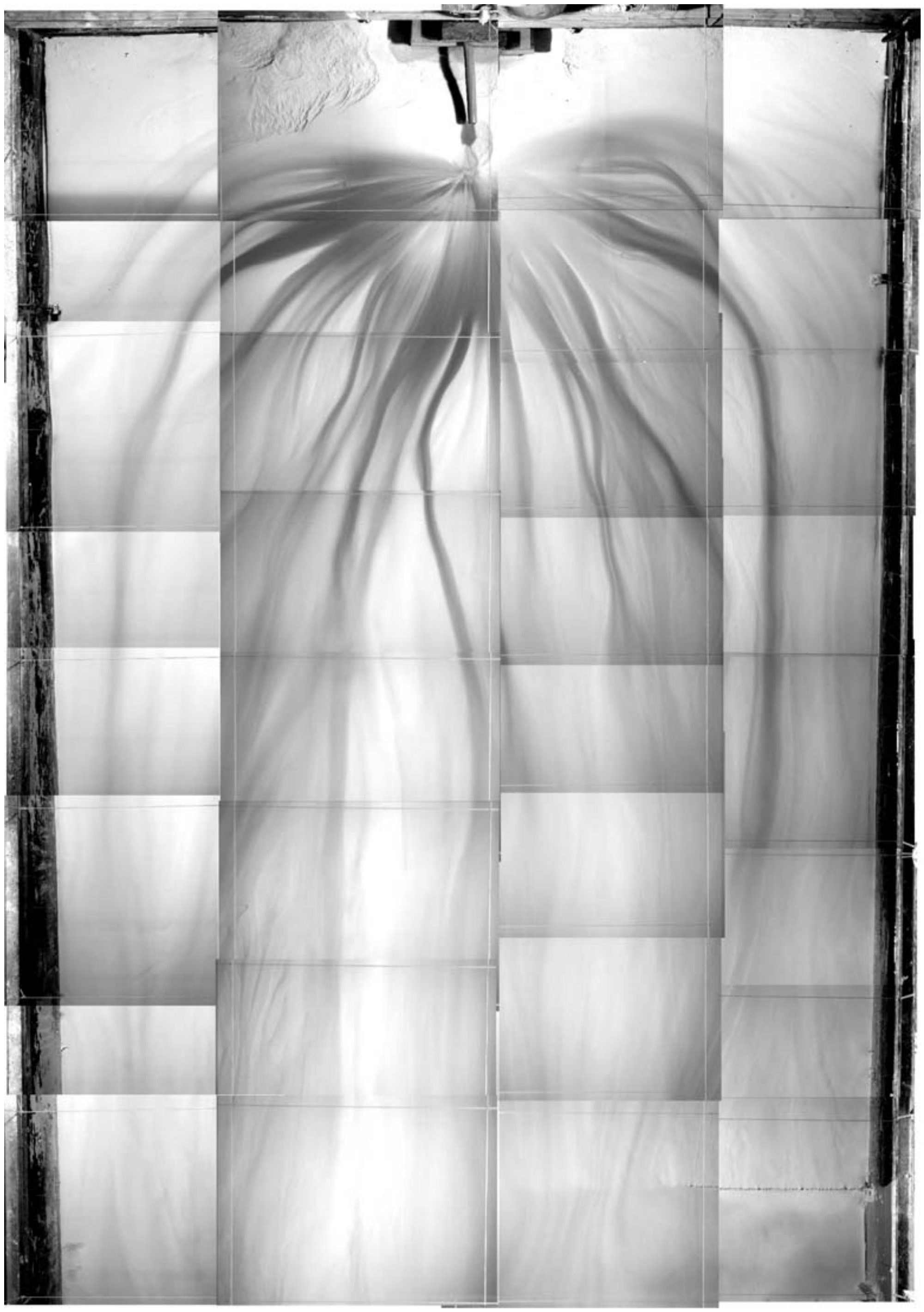

Figure 9a

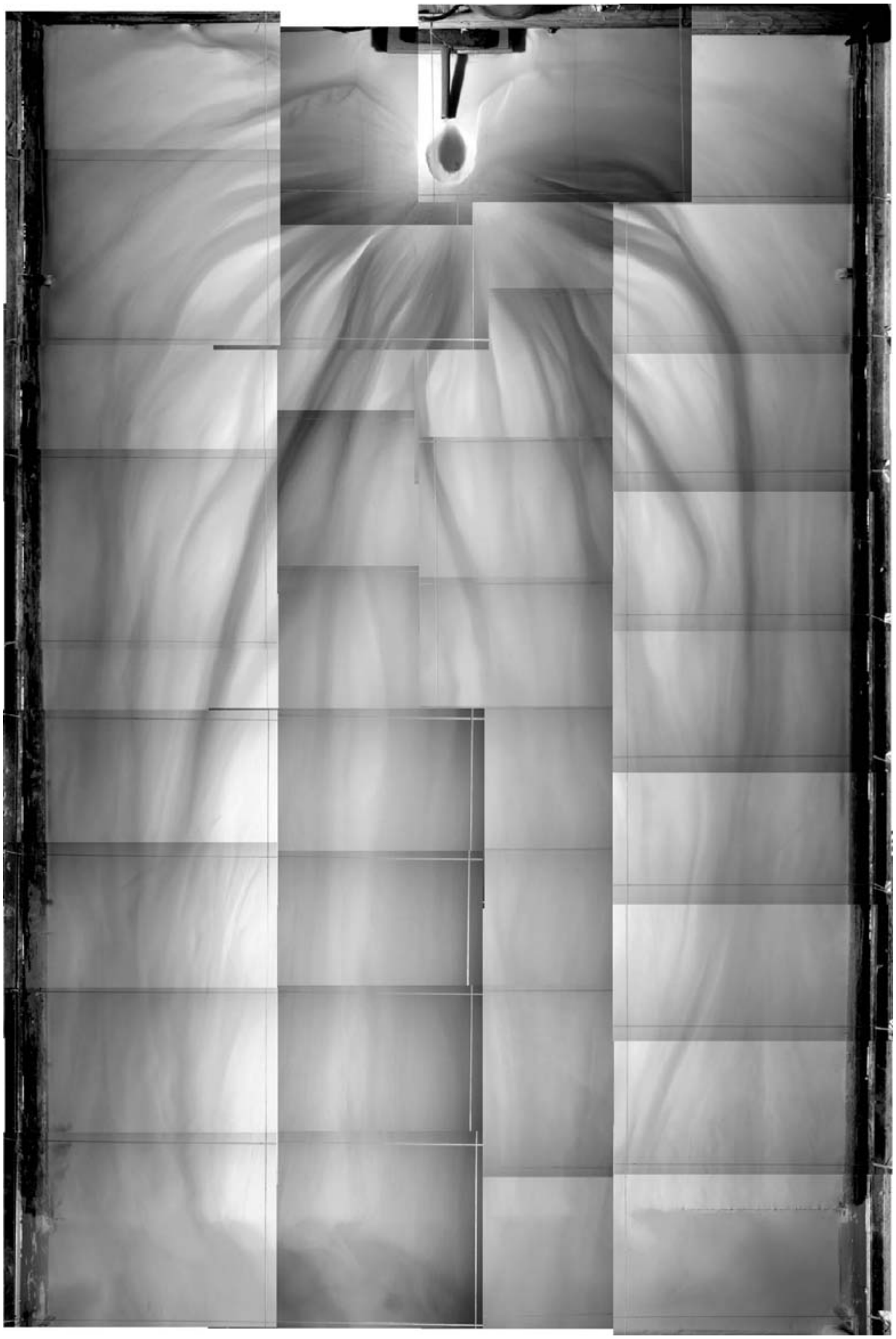

Figure 9b

Figure 10

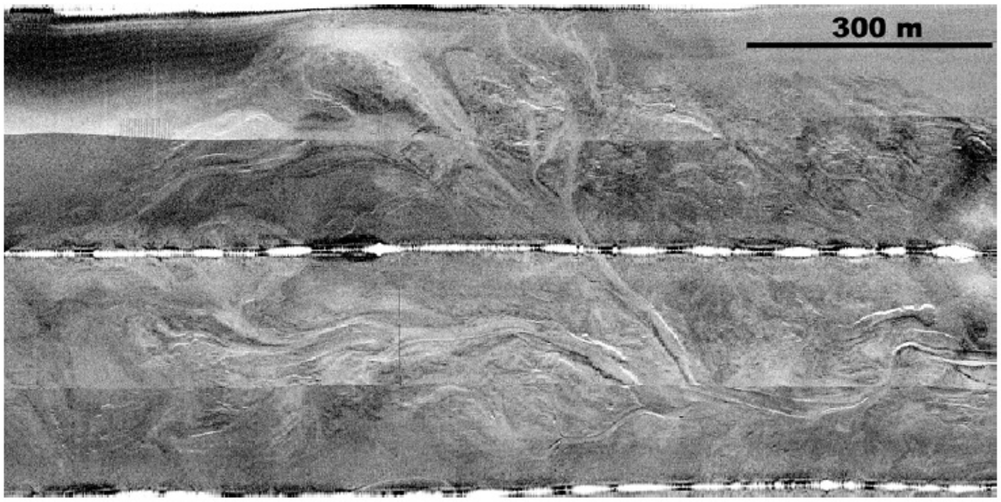


Figure 11

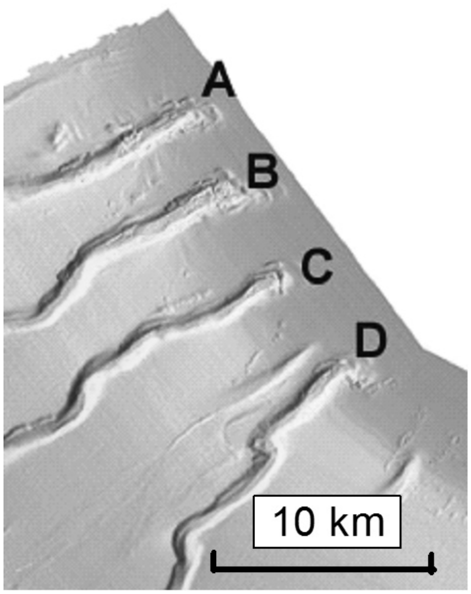


Figure 12